Sensing and Bio-Sensing Research 7 (2016) 146–152

Contents lists available at ScienceDirect

Sensing and Bio-Sensing Research

journal homepage: www.elsevier.com/locate/sbsr

Self-assembly of silver nanoparticles and bacteriophage

Santi Scibilia [a,*], Germana Lentini [b], Enza Fazio [a], Domenico Franco [b], Fortunato Neri [a], Angela Maria Mezzasalma [a], Salvatore Pietro Paolo Guglielmino [b,*]

[a] Department of Mathematical and Computer Sciences, Physical Sciences and Earth Sciences (MIFT), Viale F. Stagno d'Alcontres 31, 98166 Messina, Italy
[b] Department of Biological and Environmental Sciences, University of Messina, Viale F. Stagno d'Alcontres 31, 98166 Messina, Italy

ARTICLE INFO

Article history:
Received 8 September 2015
Accepted 3 February 2016

Keywords:
Phage display
Silver nanoparticles
Self-assembly
Hybrid architecture
Raman spectroscopy

ABSTRACT

Biohybrid nanostructured materials, composed of both inorganic nanoparticles and biomolecules, offer prospects for many new applications in extremely diverse fields such as chemistry, physics, engineering, medicine and nanobiotechnology. In the recent years, Phage display technique has been extensively used to generate phage clones displaying surface peptides with functionality towards organic materials. Screening and selection of phage displayed material binding peptides has attracted great interest because of their use for development of hybrid materials with multiple functionalities. Here, we present a self-assembly approach for the construction of hybrid nanostructured networks consisting of M13 P9b phage clone, specific for *Pseudomonas aeruginosa*, selected by Phage display technology, directly assembled with silver nanoparticles (AgNPs), previously prepared by pulsed laser ablation. These networks are characterized by UV–vis optical spectroscopy, scanning/transmission electron microscopies and Raman spectroscopy. We investigated the influence of different ions and medium pH on self-assembly by evaluating different phage suspension buffers. The assembly of these networks is controlled by electrostatic interactions between the phage pVIII major capsid proteins and the AgNPs. The formation of the AgNPs-phage networks was obtained only in two types of tested buffers at a pH value near the isoelectric point of each pVIII proteins displayed on the surface of the clone. This systematic study allowed to optimize the synthesis procedure to assembly AgNPs and bacteriophage. Such networks find application in the biomedical field of advanced biosensing and targeted gene and drug delivery.

1. Introduction

The controlled assembly of bio-hybrid nanostructured materials is an emerging research area due to their potential applications in bioengineering, biosensing and biomedical research. Among the wide variety of biological scaffolds, filamentous bacteriophages have recently attracted much attention for the development of accurately positioned nano-biotemplates, since the phage particle can be modified to form hetero-complexes with organic or inorganic nanomaterials. Ultimately, filamentous bacteriophage M13 represent attractive alternatives to antibodies or synthetic peptides, for developing new nanobiohybrid materials [1–4], due to their robustness, resistance to heat and to many organic solvent (such as 50% methanol [5] and 30% DMSO [6]) acid and alkali as well as a low-cost production [7,8]. Phage display is a high-throughput biotechnique that allows the presentation of exogenous peptides on the surface of one filamentous phage. This technology involves the introduction of exogenous peptide sequences into a location in the genome of the phage capsid proteins such as pVIII and pIII [9]. Thus, the main advantage of phage display is the enormous diversity of variant peptides that can be represented. Random phage libraries, in fact, include billion phage clones expressing on their surface more than 10^{12}–10^{14} different peptides [10]. The library is used to select specific phage clones that interact with particular targets, generating molecular probes with high affinity and selectivity [11–14].

More recently, novel strategies were developed to functionalize gold and silver nanoparticles with different Raman reporter molecules for targeting specific ligands such as peptides, proteins, antibodies, Deoxyribonucleic acid (DNA) and antibody fragments [15–19]. Nevertheless, some drawback still remain such as the availability to identify selectively and with high reproducibility probes that can act like SERS nanotags for the recognition of target cells. Taking into account the above described properties, phage-metallic nanoparticles networks are considered appropriate systems to integrate the unique signal-reporting properties of the metallic nanoparticles while preserving the biological properties of phages [20]. The surface of each filamentous bacteriophage *M*13 virus consists of about 2700 copies of a major coat protein which package a single-stranded circular viral DNA into a rod with a total length of 880 nm and a diameter of 6.6 nm [21]. This major coat protein is a charged α-helix consisting of 50 residues, and constitutes the bulk of the

* Corresponding authors.
E-mail addresses: sscibilia@unime.it (S. Scibilia), sguglielm@unime.it (S.P.P. Guglielmino).

http://dx.doi.org/10.1016/j.sbsr.2016.02.002

total charge on the virus [22]. Approximately six of the 50 residues (and the amino terminus) are solution accessible and contribute to the surface charge on *M*13. By changing the pH, change the protonation states of the amino acids on the virus major coat protein, thereby modifying the surface charge density [21].

Clearly the coat protein has the ability to adopt its conformation, which allows the protein to exist in distinctly different environments, such as the phage filament, the I form phage, the S-form phage, and the membrane-bound form [23]. This is possible because of the amphipathic nature of the coat protein so that it can have both hydrophobic and hydrophilic interactions with its environment. This property gives the protein a large conformational space that allows very flexible protein aggregational schemes.

In this work, the influence of different phage suspension buffers (i.e. the influence of different ions and medium pH) on the self-assembly of AgNPs and bacteriophage are studied in order to find the appropriate conditions to favor the formation of the AgNPs-phage complex. The silver nanoparticles were prepared using the pulsed laser ablation technique in a confining liquid. This is a chemically simple and clean synthesis method to obtain, in a one step top-down procedure, size controlled AgNPs dispersed in water. The intrinsic ability to produce stable species without the a priori need for any aggressive chemicals, like reducing or capping agents, makes laser ablation in liquids particularly attractive as an biocompatible technique, allowing to obtain AgNPs useful for biomedical applications, as that reported in this paper. On the overall, the results obtained show that an appropriate control of the electrostatic interactions between the phage pVIII major capsid proteins and the Ag nanoparticles determines the AgNPs-phage complex formation.

2. Materials and methods

2.1. Ag nanoparticles preparation

Colloidal solutions of Ag nanoparticles were prepared by pulsed laser ablation of a high purity (99.9%) silver target immersed in distilled water, using the second harmonic (532 nm) of a neodymium-doped yttrium aluminum garnet (Nd:YAG) laser (model New Wave Mod. Tempest 300) operating at 10 Hz repetition rate with a pulse width of 5 ns [24,25]. The target was irradiated at the laser fluence of 1 J/cm^2 and for an ablation time of 20 min.

2.2. Phage clone

P9b phage clone display the foreign peptide QRKLAAKLT [13], that represents a specific and selective probe for *Pseudomonas aeruginosa*, was derived from a M13 pVIII-9aa phage peptide library (kind gift of Prof. F. Felici) through previously described affinity-selection procedures [13]. A total estimated isoelectric point value (p*I*) of 6.3. of P9b phage clone was calculated by using "compute MW/pI," present on the proteomics server of the Swiss Institute of Bioinformatics Expert Protein Analysis System (ExPASy). The phage- displayed peptide P9b was chosen as a prototype for optimize the synthesis procedure to assembly AgNPs and bacteriophage.

2.3. Phage suspension buffers

In order to evaluate the influence of phage suspension buffer on the phage assembly with silver nanoparticles, different pH and ion-type buffers were used:

Phosphate Buffer (*PB**) *0.2 M pH 5.86.* Potassium phosphate monobasic anhydrous (22.4 g/l, Lickson) and sodium phosphate dibasic heptahydrate (3.49 g/l, Sigma-Aldrich) were mixed and solubilized in ultrapure water. The final pH was 5.86.

Phosphate Buffer (*PB**) *0.2 M pH 7.23.* Potassium phosphate monobasic anhydrous (9.36 g/l, Lickson) and sodium phosphate dibasic heptahydrate (32.73 g/l, Sigma-Aldrich) were mixed and solubilized in ultrapure water. The final pH was 7.23.

Phosphate Buffered Saline (*PBS*) *0.01 M pH 7.18.* Potassium phosphate monobasic (0.2 g/l, Lickson), sodium phosphate dibasic (1.15 g/l, Sigma-Aldrich), sodium chloride (8 g/L, Applichem) and potassium chloride (0,2 g/L, AnalytiCals Carlo Erba) were mixed and solubilized in ultrapure water. The final pH was 7.18.

Tris-buffered saline (*TBS*) *pH 5.18 and pH 7.02.* Tris hydrochloride (7.88 g/l, Euroclone) and sodium chloride 140 mM (8.77 g/L, Applichem) were mixed and solubilized in ultrapure water. The pH was adjusted with hydrogen chloride 5 N in order to give the final pH values of 5.18 and 7.02.

2.4. Phage-AgNPs networks preparation

The phage-AgNPs networks were prepared according to the procedure described by Lentini et al. [14]. Silver nanoparticles were incubated with the phage clone resuspended in different buffers (title of $5 \cdot 10^{11}$ pfu/ml) in a 4:1 ratio at 30 °C in orbital shaking at 320 rpm (KS130 Basic IKA) over night. In order to separate the AgNPs-phage network from the unbounded phage and free silver, networks were purified by centrifugation at 20,800 ×g for 30 min and resuspended in 5 ml of their respective buffers. The complexes were stored at 4 °C until utilization.

2.5. Samples characterization

The UV–vis absorption response of the Ag nanostructures was investigated, in the colloidal phase immediately after the ablation process, by means of a Perkin-Elmer Lambda 750 UV–vis spectrometer in the 190–1100 nm range. Further, the Ag sample morphology was investigated by means of Transmission Electron Microscopy (TEM) measurements. The TEM images were taken on appropriately dried solutions by a JEOL JEM-2010 microscope, operating at an acceleration voltage of 200KV and equipped with a Gatan 794 Multi-Scan CCD camera. A fraction of the AgNPs-phage colloidal complex was deposited on carbon substrates to carry out Scanning Electron Microscopy (SEM) characterization. SEM images were taken by a scanning electron microscope (Merlin; model ZEISS-Gemini 2) operating at an accelerating voltage of 5 kV. Micro-Raman spectroscopy measurements were carried out by means of an Horiba XploRa spectrometer equipped with an Olympus BX40 microscope, a Peltier cooled charge coupled device (CCD) sensor

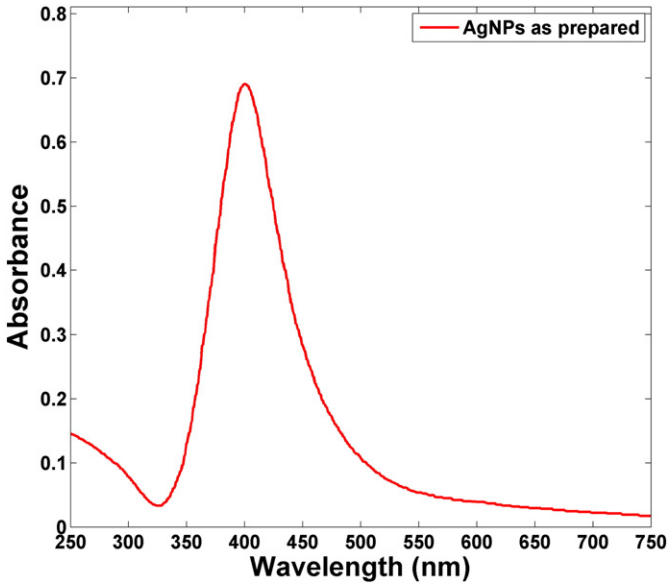

Fig. 1. Optical absorption response of Ag nanoparticles prepared in water.

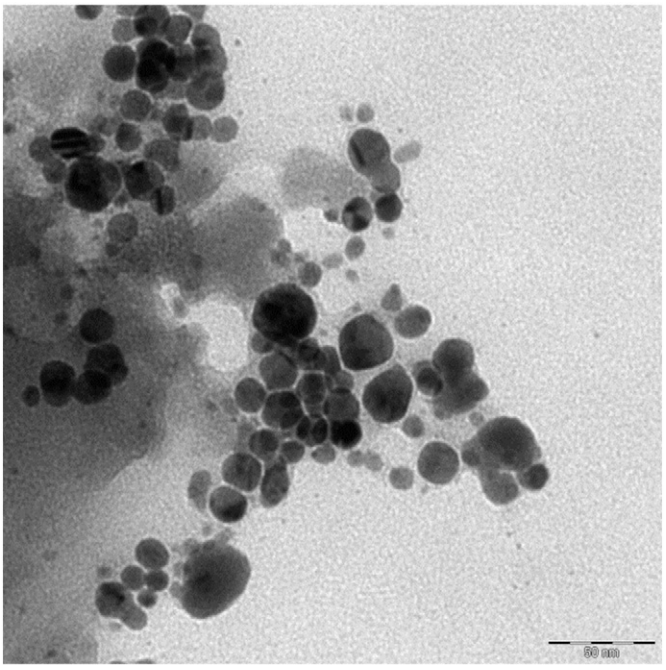

Fig. 2. TEM image of the Ag NPs.

and a 532 nm (2.33 eV) laser as the excitation source. An acquisition time of 100 s allowed a sufficient signal/noise (S/N) ratio.

2.6. Result and discussions

UV–vis optical absorption spectra of Ag nanocolloids show a well-defined absorption band (Fig. 1). The observed absorption band, is ascribed to the surface plasmon resonance (SPR) contribution, centered at 400 nm.

The Ag morphology was investigated by TEM imaging (Fig. 2). The sample consists of nearly spherical nanoparticles smaller than 20 nm in diameter. Some spherical agglomerations of about 50 nm are also evident. The observed nanoparticles overlapping could be dependent on the TEM sample preparation itself (i.e. drying a colloidal solution droplet on a microscopy grid).

In order to assess the influence of phage suspension buffer on the phage assembly with silver nanoparticles, different pH and ion-type buffers were evaluated.

Firstly, the stability of silver nanoparticles in the used buffers was evaluated by optical absorption spectroscopy in the UV–Vis region (Fig. 3).

The optical absorbance intensity value of AgNPs SPR peak decreases significantly when the Ag NPs are dispersed in the PB* buffer solution at the pH value 7.23 and it is totally absent when a solution with a pH value of 5.86 is used. The disappearance of the Ag marker indicates that no Ag nanoparticles remain in suspension. A high level of silver precipitates was seen in the glass vessels, probably due to the formation of sparingly soluble silver salts on the particle surface.

A similar behavior is observed for the Ag nanoparticles dispersed in PBS (whose pH is 7.18): only a slight hint of the SPR signal is evident. Finally, the SPR feature is totally absent in TBS. On the overall, it emerges that the optical absorbance reduction/absence of the SPR signal is probably due to the formation of sparingly soluble silver salts on the particle surface. In fact the ions present in the buffer solutions, such as sodium (Na^+), potassium (K^+), chloride (Cl^-) and phosphate (PO_4^{3-}), complex with the AgNPs resulting in nanoparticles aggregation and precipitation. This phenomenon is usually explained as resulting from the screening of electrostatic repulsions between the nanoparticles [26,27].

Taking into account these results, silver nanoparticles were incubated with the phage clone resuspended in the different buffers. In Fig. 4 are shown the optical absorption spectra of AgNPs-P9b networks in the different ion-type buffers and, for the same buffer, at different pH values.

The most relevant evidences are that the AgNPs does not totally precipitate in the presence of bacteriophage as well as an agglomeration process occurs between the species in solutions.

The spectrum of AgNPs-P9b PB* buffer solution, (see Fig. 4a), show a low visible contribution in the 250–270 nm range, due to the aromatic residues of phage [28,29] and the well-known SPR band centered at 405 nm, even if with a significantly reduced intensity values. Moreover, the SPR contribution asymmetrically widens with respect to that observed for the as prepared water Ag NPs. This behavior seems to be partially affected by the pH values of the PB* buffer solution.

In Phosphate Buffered Saline (PBS) 0.01 M pH 7.18 than in Tris-buffered saline (TBS) pH 5.18 and 7.02, a yellowish colored solution is obtained after overnight incubation at 30 °C of P9b with AgNPs.

The SPR lineshapes of the AgNPs-P9b networks in PBS and TBS (see Fig. 4b,c) show very similar behaviors to that observed in PB* (Fig. 4a),

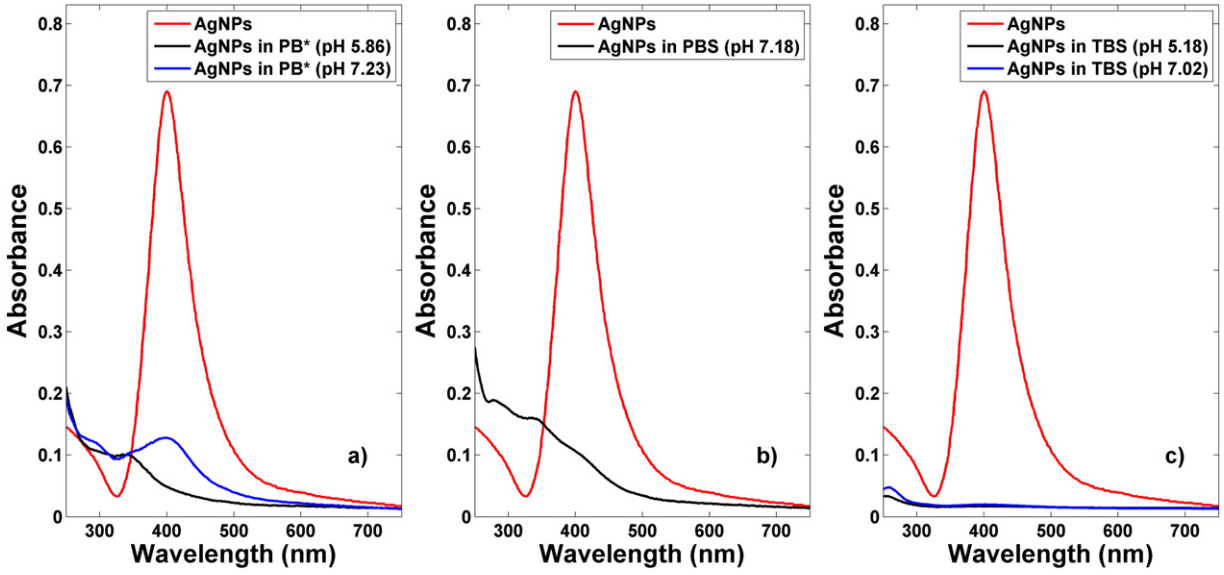

Fig. 3. Absorption spectra of the Ag NPs in different ion-type buffers and, for the same buffer, at different pH values.

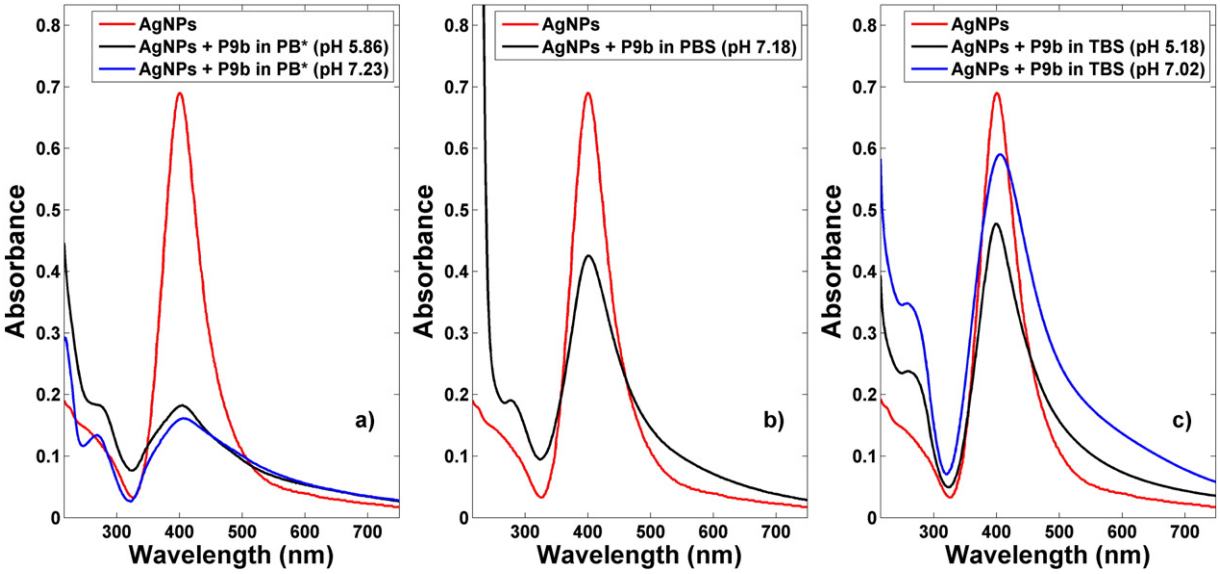

Fig. 4. Absorption spectra of AgNPs-P9b networks in the different ion-type buffers and, for the same buffer, at different pH values.

even if the SPR broading effect is less evident. Moreover, also in this case we see the phage signals around 270 nm.

Comparing these features with the behavior shown in Fig. 3, the most relevant evidence is the persistence of AgNPs SPR peak, which is significantly decreased in the absence of the phage. AgNPs do not totally precipitate in the presence of bacteriophage and, indirectly, it indicates an interaction between phage and AgNPs, maintaining them in suspension. This behavior seems to be partially affected by the pH values of the buffer solution.

This effect appears to be stronger for AgNPs in PBS and TBS respect to the ones in PB* and it is attributed to the different ionic species present in the buffers. On the overall, the optical absorption response in the different ion-type buffers and pH values is influenced by the different ions present and by the fluctuations in the surrounding ion clouds [30].

Polyelectrolytes in aqueous solution are coated by a condensed layer of mobile oppositely charged counterions [21]. Because of their polyelectrolyte nature, M13 and other filamentous viruses can be complexed by different ions, changing the spatial distributions of charges on their surfaces. In particular, pVIII major coat proteins constitute the bulk of the total charge on the virus [31].

Changes in the phage surface charge dramatically affect its ability to assemble procapsids, as reported by Parent et al. [32]. They demonstrated that P22 phage capsid assembly is driven by multiple protein–protein electrostatic interactions of viral subunits during the assembly

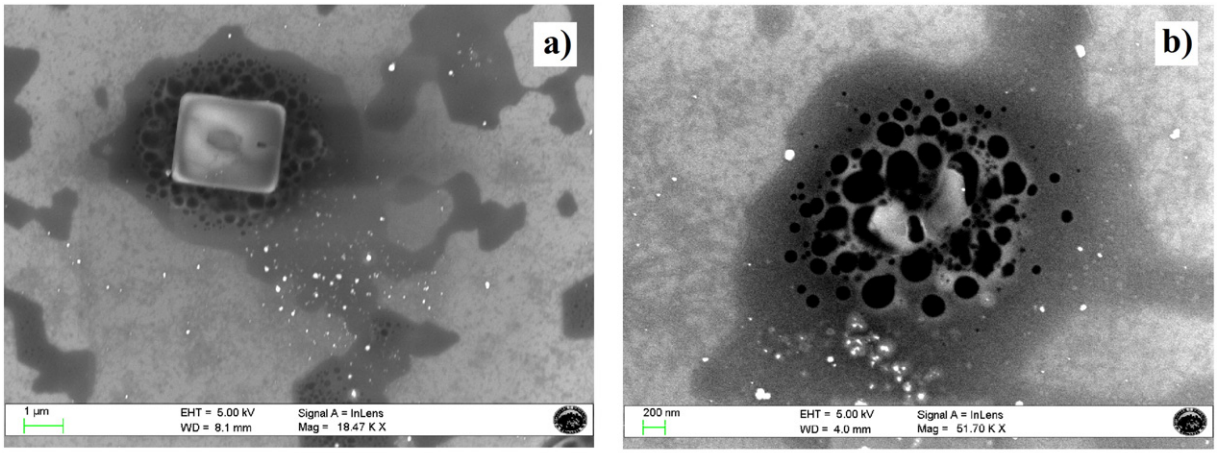

El	AN	Series	unn. [wt.%]	C norm. [wt.%]	C Atom. [at.%]	Error(1Sigma) [wt.%]
Si	14	K-series	104,52	73,57	76,37	4,92
Ag	47	L-series	25,61	18,03	4,87	1,77
C	6	K-series	7,82	5,50	13,35	1,30
O	8	K-series	2,07	1,45	2,65	0,47
N	7	K-series	1,77	1,24	2,59	0,46
Cl	17	K-series	0,28	0,20	0,16	0,06
Total:			142,06	100,00	100,00	

Fig. 5. SEM image of AgNPs-P9b networks in TBS.

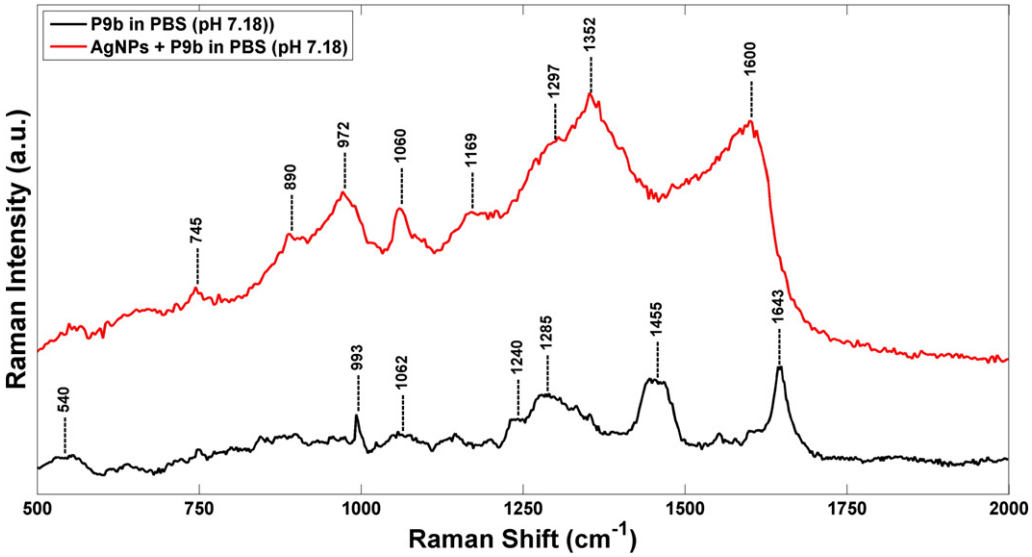

Fig. 6. Raman spectra of AgNPs-P9b networks in PBS (pH 7.18).

process. The concentration and type of salt was found to be crucial for proper association, nucleation and elongation of correctly assembled procapsids. Anionic interactions are necessary and important for mediating P22 procapsid assembly. Furthermore, anions could alter formation of salt bridges between coat and scaffolding proteins or change solvent hydration of the individual proteins.

The importance of salt–bridge interactions in stabilizing proteins varies and appears to be highly dependent upon factors such as the screening of the charges by solvent, the cost of desolvating the charged groups to form these bridges, and the relative flexibility of the side chains involved in the ion pair [33].

Furthermore, the pVIII protein surface charge density can be controlled by changing the pH of the system which, in this work, is appropriately changed in order to obtain a pH value in an interval around the isoelectric point pI of P9b phage. As reported before, for the P9b phage the pVIII protein pI value is 6.3, this means that the protein surface charge is positive at pH below pI, for example in the case of TBS pH 5.18, and negative at pH above pI, such as for TBS at pH 7.02, but in both cases we notice a similar behavior. This result suggests that the assembly of silver nanoparticles onto phage is not only directed by opposite-charge interaction between silver nanoparticles and bacteriophage, but an important role is related to the different types of ions present in the buffer. The electrostatic interactions between silver nanoparticles and bacteriophage are governed by the Brownian motion of the ions in the buffer solution, that act like attractor sites, by creating salt bridge and promoting the formation of AgNPs-phage networks.

The occurred formation of the networks, consisting of entire bacteriophage structure directly assembled with AgNPs, was evidenced carrying out SEM/EDX measurements. Particularly closed-packed Ag-phage nanostructures were formed on the assembled phage films on all the micrometer-length scale investigated, as shown in Fig. 5. Most of the

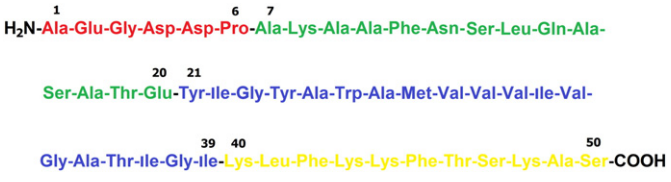

Fig. 7. Schematic showing the primary structure and domain organization of the pVIII major coat protein in phage M13. Red: acid domain (1–6); Green: amphipathic domain (7–20); Blue: hydrophobic domain (21–39); Yellow: basic domain (40–50).

AgNPs are in the regions in which the EDX probe shows the presence of nitrogen, carbon and oxygen species as well as atomic species typical of salts. This result indicates that the phage structures are decorated to the AgNPs and in proximity of the salts.

The Ag-phage networks were also characterized carrying out Raman measurements. No Raman features typical of the phage in the 600–2000 cm^{-1} range was observed for the Ag-phage network in PB*. This is probably due to an excess of phosphate ions present in solution that led to the formation of unstable networks.

In Fig. 6 are shown the Raman spectra of P9b phage and AgNPs-P9b networks in PBS (pH 7.18). The Raman spectrum of phage is characterized by some contributions located at 993, 1285 and 1643 cm^{-1}, attributed to the stretching mode of amide and the peaks centered at 540 and 1455 cm^{-1}, ascribed to polar and aromatic residues of phage coat proteins [34,35].

In particular, the contribute at 540 cm^{-1} is related to ν(S–S) trans-gauche-trans mode of amino acid cysteine. The wild-type sequences of M13 major coat proteins do not contain cysteines, whereas pIII, pVII, and pIX have internal cysteines that play important roles in structure formation via disulfide bonds [36]. Moreover, the phage Raman spectrum is characterized by a barely visible band at 1240 cm^{-1}, due to amide III random coil, and by a narrow peak at 1643 cm^{-1}, attributed to the major capsid protein (pVIII) α-helix secondary structure [37–39].

The AgNPs–P9b network shows some differences respect to the P9b phage. We observe a significant shift of the Raman features associated to the protein contributions and the appearance of new Raman features, centered at around 745, 890, 972, 1169, 1297, 1352 and 1600 cm^{-1}). Moreover, with respect to the P9b phage Raman spectrum, it is very intense the contributions at about 1060 cm^{-1}, referred to the PO^{2-} stretching mode of packaged ssDNA phage [40] and the peak at 745, 890 and 972 and at 1352 cm^{-1}, ascribed to the symmetric breathing of tryptophan, C-C and C-N stretching mode of amide. These spectral changes depend on the orientation and the distance of the molecules from the surface of the metal nanostructures [41]. We remember that the M13 filamentous bacteriophage coat is a symmetric array of several thousand α-helical major coat proteins (pVIII) that surround the DNA core. The structure of the pVIII major coat protein has been studied by different methods [42,43], which collectively provide many details about main chain and side chain conformations, subunit orientation, and filament architecture. The sequence of pVIII can be divided into four functional domains [22]: (*i*) an acid (1–6) and an amphipathic domain (7–20) on the N-terminus; (*ii*) a hydrophobic (21–39) and a basic domain (40–50) located near the C-terminus (see Fig. 7). Moreover, as

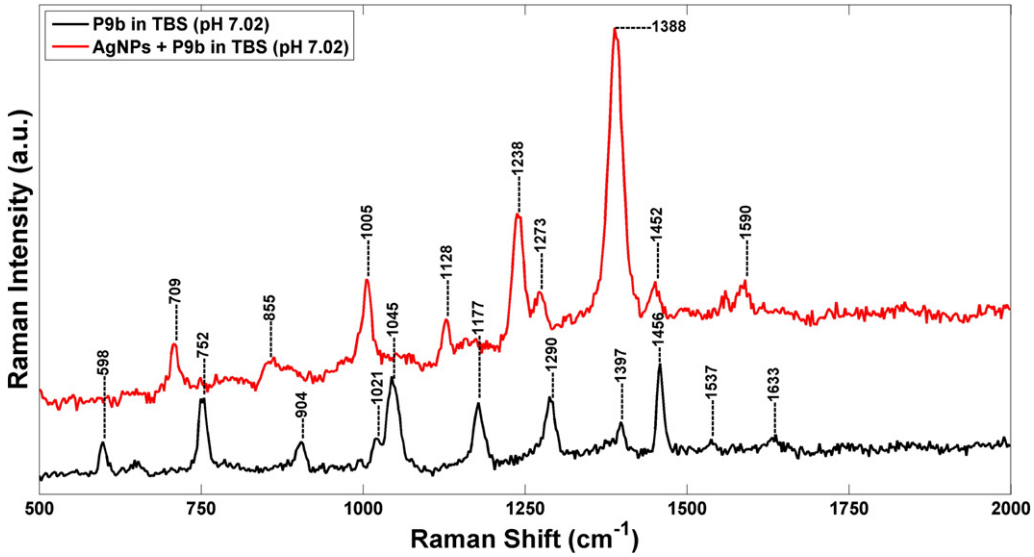

Fig. 8. Raman spectra of AgNPs-P9b networks in TBS (pH 7.02).

known from literature [44,45], Tyr 21 and Tyr 24 are located in a loop region while Phe 26 is positioned in an α-helix tract.

Approximately six of the 50 residues (and the amino terminus NH_2) are solution accessible and contribute to the surface charge on M13. By changing the pH or the ions in buffer solution, we change the protonation states of the amino acids on the virus major coat protein, thereby modifying the surface charge density [21] This property gives the protein a large conformational space that allows very flexible protein aggregational schemes. The transition between the different conformations depends on pH and salt concentration.

In this contest the Raman spectral changes, observed in presence of the Ag NPs, are mainly index of stretching modes deformation of tyrosine and phenylalanine residues of the hydrophobic region of the Tyr 21, Tyr 24 and Phe 26 major capsid proteins which are located near the C-terminus of the pVIII proteins [46]. On the overall, these Raman spectral changes suggest the occurred phage direct interaction with AgNPs [47], preserving the binding activity of the engineered peptides displayed on the N-terminus of the same major coat proteins.

In Fig. 8 are shown the Raman spectra of P9b phage and AgNPs-P9b networks in TBS (pH 7.02). In TBS, the Raman spectrum of phage is similar to one observed in PBS. However, some features related to the CH_2OH groups stretching vibration of polar amino acids serine and threonine at 1045 cm^{-1} [48] and to the vibrational modes of the nucleotide bases of packaged ssDNA located at 598 and 1290 cm^{-1} [40] are more evident. Furthermore, the folding variation of phage coat proteins in TBS buffer is confirmed by the presence of a peak located at 904 cm^{-1}, assigned to the variations in the secondary structures of proteins (CH_2/CH_3 deformations as scissoring, wagging, twisting, and rocking).

The main differences between the Raman spectra of AgNPs-P9b complex and P9b in TBS are: (*i*) the shift of the phenylalanine contribution from 1456 cm^{-1} down to 1452 cm^{-1}; (*ii*) the appearance of new Raman peaks at 1005 and 1590 cm^{-1}, ascribed to asymmetric and symmetric ring breathing modes of phenylalanine [47]; (*iii*) the appearance of new contributes at 709 and 855 cm^{-1}, assignable to tyrosine residues [49,50]; (*iv*) the appearance of some peaks related to protein stretching modes (at 1128, 1238, 1273 and 1388 cm^{-1}).

These dynamic structural changes indicate the binding of silver nanoparticles mainly on the aromatic side chains of tyrosine and phenylalanine residues. In particular, three important residues (Tyr 21, Tyr 24 and Phe 26), located in a highly hydrophobic segment of the pVIII proteins, are involved in the assembly of bacteriophage and AgNPs. Furthermore, the appearance of a new peak at 1273 cm^{-1}, which is assignable to CH α-helix rocking, confirm the folding variation of the α-helix portion of the hydrophobic domain where the phenylalanine residue 26 is located [46,51]. In this way, the engineered peptides on N-terminal portions of the PVIII remain available for a specific and selective target-binding.

A similar approach was adopted by Souza et al. that studied the effect of cis- and trans-acting factors on the bottom-up assembly of Au nanoparticles (AuNPs) with either native or mutant bacteriophage [52]. The cis-acting factor consists of a peptide extension displayed on the pVIII that mutates the phage, while the trans-acting factor is represented by pH variation of the medium. A stable and spontaneous organization of these hydrogels was achieved by turning the pH, and therefore controlling phage surface charge, or by changing the composition of the phage pVIII. However, this Au-phage assembly is a combination of citrate replacement coupled with electrostatic interaction between the charged residues on the pVIII and AuNPs. So the interaction between nanoparticles and phage are mainly governed by the opposite-charge interaction, differently from our system in which the different types of ions of the medium have a fundamental role on the assembly.

3. Conclusions

M13 bacteriophage can serve as a versatile and multifunctional material building block due to the ease of its genetic manipulation and its monodisperse filamentous shape. We have investigated some of the variables that influence the organization and assembly of phage with silver nanoparticles. Our result suggests that, the AgNPs-phage assembly are not only directed by opposite-charge interaction, but a significant role is played by the pH and the ion-type buffer solution. We found that the organization and assembly of laser prepared AgNPs and phage was favorite significantly at pH above the phage pI and using saline buffer (with presences of Na^+ and Cl^-) that form saline bridge between AgNPs and phage. The streamlined methodology, reported in this study, may serve as a complementary approach to understand and to gain control on the assembly of active phage-nanoparticles system. These networks could find application in the biomedical field of advanced biosensing, tissue engineering, bioelectronic systems and targeted gene and drug delivery.

Acknowledgements

This work was partially funded by Italian Ministry of Education, University and Research (MIUR) by means of the national Program

PON R&C 2007-2013, project “Hyppocrates–Sviluppo di Micro e Nano-Tecnologie e Sistemi Avanzati per la Salute dell'uomo (PON02 00355)”. Authors also gratefully acknowledge A.B.A.L. onlus Messina (Italy) (http://abalmessina.it/) for the use of the XploRA Raman spectrometer and Prof. Franco Felici for the kind gift of clone selection from his phage-display libraries.

References

[1] C.M. Soto, B.R. Ratna, Virus hybrids as nanomaterials for biotechnology, Curr. Opin. Biotechnol. 21 (2010) 426–438.
[2] A. Merzlyak, S.W. Lee, Engineering phage materials with desired peptide display: Rational Design sustained through natural selection, Bioconjug. Chem. 20 (2009) 2300–2310.
[3] T. Yata, K.Y. Lee, T. Dharakul, S. Songsivilai, A. Bismarck, P.J. Mintz, A. Hajitou, Hybrid Nanomaterial Complexes for Advanced Phage-guided Gene Delivery, Mol. Ther. Nucleic Acids 3 (2014) e185.
[4] B. Bakhshinejad, M. Sadeghizadeh, Bacteriophages and development of nanomaterials for neural regeneration, Neural. Regen. Res. 15 (2014) 1955–1958.
[5] E. Royston, S.Y. Lee, J.N. Culver, M. Harris, Characterization of silica-coated tobacco mosaic virus, J. Colloid Interface Sci. 298 (2006) 706–712.
[6] M.A. Bruckman, G. Kaur, L.A. Lee, F. Xie, J. Sepulveda, R. Breitenkamp, X.F. Zhang, M. Joralemon, T.P. Russell, T. Emrick, Q. Wang, Surface modification of tobacco mosaic virus with “click” chemistry, Chembiochem 9 (2008) 519–523.
[7] V.A. Petrenko, G.P. Smith, Phage from landscape libraries as substitute antibodies, Protein Eng. 13 (2000) 101–104.
[8] V.A. Petrenko, V.J. Vodyanoy, Phage display for detection of biological threat agents, J. Microbiol. Methods 53 (2003) 243–252.
[9] G.P. Smith, V.A. Petrenko, Phage display, Chem. Rev. 97 (1997) 391–410.
[10] H. Qi, H. Lu, H.-J. Qiu, V. Petrenko, A. Liu, Phagemid vectors for phage display: properties, characteristics and construction, J. Mol. Biol. 417 (2012) 129–143.
[11] M.A. Arap, Phage display technology — applications and innovations, Genet. Mol. Biol. 28 (2005) 1–9.
[12] S. Carnazza, G. Gioffrè, F. Felici, S. Guglielmino, Recombinant phage probes for Listeria monocytogenes, J. Phys. Condens. Matter 19 (2007) 395011 (13 pp.).
[13] S. Carnazza, C. Foti, G. Gioffrè, F. Felici, S. Guglielmino, Specific and selective probes for *Pseudomonas aeruginosa* from phage-displayed random peptide libraries, Biosens. Bioelectron. 23 (2008) 1137–1144.
[14] G. Lentini, E. Fazio, F. Calabrese, L.M. De Plano, M. Puliafico, D. Franco, M.S. Nicolò, S. Carnazza, S. Trusso, A. Allegra, F. Neri, C. Musolin, S. Guglielmino, Phage–AgNPs complex as SERS probe for U937 cell identification, Biosens. Bioelectron. 74 (2015) 398–405.
[15] Y. Zhang, H. Hong, D.V. Myklejord, W. Cai, Molecular imaging with SERS-active nanoparticles, Small 7 (2011) 3261–3269.
[16] J.V. Jokerst, Z. Miao, C. Zavaleta, Z. Cheng, S.S. Gambhir, Affibody-functionalized gold-silica nanoparticles for Raman molecular imaging of the epidermal growth factor receptor, Small 7 (2011) 625–633.
[17] F. Gao, J. Lei, H. Ju, Label-free surface-enhanced Raman spectroscopy for sensitive DNA detection by DNA-mediated silver nanoparticle growth, Anal. Chem. 85 (2013) 11788–11793.
[18] J. Neng, M.H. Harpster, W.C. Wilson, P.A. Johnson, Surface-enhanced Raman scattering (SERS) detection of multiple viral antigens using magnetic capture of SERS-active nanoparticles, Biosens. Bioelectron. 41 (2013) 316–321.
[19] J. Baniukevic, I.H. Boyaci, A.G. Bozkurt, U. Tamer, A. Ramanavicius, A. Ramanaviciene, Magnetic gold nanoparticles in SERS-based sandwich immunoassay for antigen detection by well oriented antibodies, Biosens. Bioelectron. 43 (2013) 281–288.
[20] N. Tawil, E. Sacher, E. Boulais, R. Mandeville, M. Meunier, X-ray photoelectron spectroscopic and transmission electron microscopic characterizations of bacteriophage–nanoparticle complexes for pathogen detection, J. Phys. Chem. C 117 (2013) 20656–20665.
[21] J.C. Butler, T. Angelini, J.X. Tang, G.C.L. Wong, Ion multivalence and like-charge polyelectrolyte attraction, Phys. Rev. Lett. 91 (2003) 028301.
[22] V.A. Petrenko, G.P. Smith, M.M. Mazooji, T. Quinn, α-helically constrained phage display library, Protein Eng. 15 (2002) 943–950.
[23] D. Stopar, R.B. Spruijt, C.J.M. Wolfs, M.A. Hemminga, Protein–lipid interactions of bacteriophage M13 major coat protein, Biochim. Biophys. Acta 1611 (2003) 5–15.
[24] E. Fazio, S. Trusso, R.C. Ponterio, Surface-enhanced Raman scattering study of organic pigments using silver and gold nanoparticles prepared by pulsed laser ablation, Appl. Surf. Sci. 272 (2013) 36–41.
[25] E. Fazio, F. Neri, Nonlinear optical effects from Au nanoparticles prepared by laser plasmas in water, Appl. Surf. Sci. 272 (2013) 88–93.
[26] D. Wang, B. Tejerina, I. Lagzi, B. Kowalczyk, B.A. Grzybowski, Bridging interactions and selective nanoparticle aggregation mediated by monovalent cations, ACS Nano 5 (2011) 530–536.
[27] I. Ojea-Jiménez, V. Puntes, Instability of cationic gold nanoparticle bioconjugates: the role of citrate ions, J. Am. Chem. Soc. 131 (2009) 13320–13327.
[28] F.X. Schmid, in: Bridgewater R. (Ed.), Encyclopedia Life Sci, Introductory Articles 2001, pp. 1–4.
[29] S.A. Overman, P. Bondr, N.C. Maiti, G.J. Thomas Jr., "Structural characterization of the filamentous bacteriophage PH75 from *Thermus thermophilus* by Raman and UV-resonance Raman spectroscopy, Biochemistry 44 (2005) 3091–3100.
[30] D.-Y. Jeon, K.H. Hwang, S.-J. Park, Y.-J. Kim, M.-K. Joo, S.-E. Ahn, G.-T. Kim, C.-H. Nam, Controlled surface adsorption of fd filamentous phage by tuning of the pH and the functionalization of the surface, J. Appl. Phys. 109 (2011) 064701.
[31] L. Makowski, M. Russel, Structure and assembly of filamentous bacteriophages, in: W. Chiu, R.M. Burnett, R.L. Garcea (Eds.), Structural Biology of Viruses, Oxford University Press, New York 1997, pp. 352–380.
[32] K.N. Parent, S.M. Doyle, E. Anderson, C.M. Teschke, Electrostatic interactions govern both nucleation and elongation during phage P22 procapsid assembly, Virology 340 (2005) 33–45.
[33] A.-S. Yang, K.A. Sharp, B. Honig, Analysis of the heat capacity dependence of protein folding, J. Mol. Biol. 227 (1992) 889–900.
[34] D. Aslanian, Gy Rontó, K. Tóth, Raman study of isolated and “in situ” T7 phage DNA: conformation and possible interaction with the proteins, Acta Phys. Acad. Sci. Hung. 53 (1982) 25–32.
[35] K.L. Aubrey, G.J. Thomas Jr., Raman spectroscopy of filamentous bacteriophage Ff (fd, M13, f1) incorporating specifically-deuterated alanine and tryptophan side chains. Assignments and structural interpretation, Biophys. J. 60 (1991) 1337–1349.
[36] W.-J. Chung, D.-Y. Lee, S.Y. Yoo, Chemical modulation of M13 bacteriophage and its functional opportunities for nanomedicine, Int. J. Nanomedicine 9 (2014) 5825–5836.
[37] J.L. Lippert, D. Tyminski, P.J. Desmeules, Determination of the secondary structure of proteins by laser Raman spectroscopy, J. Am. Chem. Soc. 98 (1976) 7075–7080.
[38] Y.A. Wang, X. Yu, S. Overman, M. Tsuboi, G.J. Thomas Jr., E.H. Egelman, The structure of a filamentous bacteriophage, J. Mol. Biol. 361 (2006) 209–215.
[39] S. Siddhanta, C. Narayana, Surface enhanced Raman spectroscopy of proteins: implications for drug designing, Nanomater. Nanotechnol. 2 (2012) 1–13.
[40] J.M. Benevides, P.L. Stow, L.L. Ilag, N.L. Incardona, G.J. Thomas Jr., Differences in secondary structure between packaged and unpackaged single-stranded DNA of bacteriophage phi X174 determined by Raman spectroscopy: a model for phi X174 DNA packaging, Biochemistry 30 (1991) 4855–4863.
[41] E. Podstawka, Y. Ozaki, L.M. Proniewicz, Part II: surface-enhanced Raman spectroscopy investigation of methionine containing heterodipeptides adsorbed on colloidal silver, Appl. Spectrosc. 58 (2004) 570–580.
[42] M.J. Glucksman, S. Bhattacharjee, L. Makowski, Three-dimensional structure of a cloning vector. X-ray diffraction studies of filamentous bacteriophage M13 at 7A resolution, J. Mol. Biol. 226 (1992) 455–470.
[43] D.A. Marvin, L.C. Welsh, M.F. Symmons, W.R. Scott, S.K. Straus, Molecular structure of fd (f1, M13) filamentous bacteriophage refined with respect to X-ray fibre diffraction and solid-state NMR data supports specific models of phage assembly at the bacterial membrane, J. Mol. Biol. 355 (2006) 294–309.
[44] M. Matsuno, H. Takeuchi, S.A. Overman, G.J. Thomas Jr., Orientations of tyrosines 21 and 24 in coat subunits of Ff filamentous virus: determination by Raman linear intensity difference spectroscopy and implications for subunit packing, Biophys. J. 74 (1998) 3217–3225.
[45] D.A. Marvin, M.F. Symmons, S.K. Straus, Structure and assembly of filamentous bacteriophages, Prog. Biophys. Mol. Biol. 114 (2014) 80–122.
[46] M. Tsuboi, K. Ushizawa, K. Nakamura, J.M. Benevides, S.A. Overman, G.J. Thomas Jr., Orientations of Tyr 21 and Tyr 24 in the capsid of filamentous virus Ff determined by polarized Raman spectroscopy, Biochemistry 40 (2001) 1238–1247.
[47] S. Stewart, P.M. Fredericks, Surface-enhanced Raman spectroscopy of amino acids adsorbed on an electrochemically prepared silver surface, Spectrochim. Acta A 55 (1999) 1641–1660.
[48] I. ur Rehman, Z. Movasaghi, S. Rehman, Series in Medical Physics and Biomedical Engineering, CRC Press, Taylor & Francis Group, 2012.
[49] M.N. Siamwiza, R.C. Lord, M.C. Chen, T. Takamatsu, I. Harada, H. Matsuura, T. Shimanoichi, Interpretation of the doublet at 850 and 830 cm-1 in the Raman spectra of tyrosyl residues in proteins and certain model compounds, Biochemistry (1975) 4870–4876.
[50] S.A. Overman, K.L. Aubrey, N.S. Vispo, G. Cesareni, G.J. Thomas Jr., Novel tyrosine markers in Raman spectra of wild-type and mutant (Y21M and Y24M) Ff virions indicate unusual environments for coat protein phenoxyls, Biochemistry (1994) 1037–1042.
[51] T.A. Roth, G.A. Weiss, C. Eigenbrot, S.S. Sidhu, A minimized M13 Coat protein defines the requirements for assembly into the bacteriophage particle, J. Mol. Biol. 322 (2002) 357–367.
[52] G.R. Souza, E. Yonel-Gumruk, D. Fan, J. Easley, R. Rangel, L. Guzman-Rojas, J.H. Miller, W. Arap, R. Pasqualini, Bottom-up assembly of hydrogels from bacteriophage and Au nanoparticles: the effect of cis- and trans-acting factors, PLoS One 3 (2008), e2242.